Three-Dimensional Rayleigh-Taylor Instability of Spherical Systems

H. Sakagami
Institute for Supercomputing Research, Recruit Company Ltd., 1-13-1 Kachidoki Chuo-ku, Tokyo 104, Japan

K. Nishihara
Institute of Laser Engineering, Osaka University, 2-6 Yamadaoka Suita, Osaka 565, Japan
(Received 19 March 1990)

A fully three-dimensional Rayleigh-Taylor instability of the pusher-fuel contact surface in a spherically stagnating system is investigated with the use of a new three-dimensional fluid code IMPACT-3D. Linear growth rates in the simulations agree quite well with analytical values which include spherical-geometry effects. Saturation amplitudes of the exponential growth and free-fall speed following the saturation are found to be, respectively, larger and faster than those of 2D simulations. Nonlinear bubble-spike structures are also studied in detail.

PACS numbers: 52.35.Py, 52.65.+z

In the stagnation phase of imploding targets in inertial-confinement fusion, a perturbation at the pusher-fuel contact surface is Rayleigh-Taylor unstable. It is important to investigate this instability since the pusher-fuel mixing[1,2] associated with the Rayleigh-Taylor instability reduces the total nuclear reaction yield to significantly lower values than those predicted by one-dimensional simulations. There have been, however, few three-dimensional calculations. We have investigated the linear and nonlinear features of the fully three-dimensional (3D) Rayleigh-Taylor (RT) instability in spherically stagnating targets through numerical simulations. The RT instability in spherical geometry is quite different from that in planar geometry because acceleration and wavelength vary in space and time. The nonlinear evolution in 3D simulations, as will be shown in this Letter, also significantly differs from that obtained by 2D simulations.

Any arbitrary perturbation of a surface wave in spherical geometry can be expanded in spherical-harmonic functions. Modes of 6, 10, and 12 are, for example, the most dominant perturbations of the nonuniformities in laser energy deposition in the case of a twelve-beam irradiation system,[3,4] such as the Gekko XII laser at Osaka University. There may exist more dangerous modes as a consequence of the competition between growth and damping, or stabilization due to such effects as viscosity, surface tension, thermal smoothing,[5] and ablative stabilization.[6] The most dangerous modes are probably much greater than 6. However, the relative importance of each of these processes and their combined effects, which determine the growth of the higher modes, are not well understood. As will be shown in this paper, saturation amplitudes of the exponential growth become of the order of the wavelength and consequently low modes have large saturation amplitudes. In addition, mode coupling of high modes also generates low modes.[7] Therefore both high and low modes could be important. At this point, it is still difficult to simulate high modes in a fully 3D spherical geometry due to the limitations of the present computer. In this paper, we investigate linear and nonlinear evolution of spherical-harmonic perturbations with relatively low mode numbers.

For 3D simulations we have developed a new fluid code, IMPACT-3D, which is a direct extension of IMPACT-2D.[8] Fully Eulerian and Cartesian coordinate systems are employed. The basic conservation equations for mass, momentum, and total energy density are numerically solved with an explicit total variation diminishing scheme.[9-13]

Initially, the pusher and ablator are assumed to have constant velocity toward the center of the target, with the fuel at rest. The shock wave then propagates through the fuel and is accelerated to the center of the target until it collides at the origin. After the collision, the shock wave is reflected and collides at the contact surface which is also accelerated to the center, and the stagnation phase begins at this time. The spatial profiles of physical values at the time when the stagnation phase begins are saved in a file as a function of radius and used as initial conditions for subsequent simulations. At the start of each simulation, a small single-mode perturbation is applied to the density profile near the contact surface, as we have done in 2D simulations,[8] with a spherical-harmonic function as follows:

$$\rho_1(r,\theta,\phi,n,m)=\rho_0(r+\delta r\, Y_n^m(\theta,\phi)), \tag{1}$$

$$\delta r=\begin{cases}\delta_0\{\frac{1}{2}\cos[2\pi(r-r_c)/w]+\frac{1}{2}\}, & |r-r_c|<\frac{1}{2}w,\\ 0, & |r-r_c|\geq\frac{1}{2}w,\end{cases}$$

where $\rho_0(r)$, δ_0, w, r_c, and $Y_n^m(z)$ are the saved density profile as a function of the radius, the initial perturbation amplitude, the perturbation width, the radius of the contact surface, and the spherical-harmonic function, respectively. The spherical-harmonic function is defined as follows:

$$Y_n^m(\theta,\phi)=\left[\frac{2n+1}{4\pi}\frac{(n-m)!}{(n+m)!}\right]^{1/2}\times P_n^m(\cos\theta)e^{im\phi}\quad(0\leq m\leq n), \tag{2}$$

TABLE I. Initial conditions and simulation parameters for 3D RT instability.

	Initial conditions			
	Radius (μm)	Density (g/cm^3)	Pressure (Mbar)	Velocity (10^6 cm/sec)
Fuel	<70	0.5	10	0
Pusher	70–108	5.0	10	15
Ablator	>108	0.5	10	15

Simulation parameters	
Grid points	$81\times81\times81$
Mesh size	1.5 μm (before stagnation)
	1.0 μm (during stagnation)
Boundary conditions	$\frac{1}{8}$ sphere (before stagnation)
	Full sphere (during stagnation)

where $P_n^m(z)$ is the Legendre function, n and m are the polar and azimuthal mode numbers, respectively, and we set $\delta_0/r_c=0.01$ and $w/r_c=0.5$ to investigate the linear growth rate of the 3D RT instability. The origin of the target is located at the center of a cubic mesh system which has $81\times81\times81$ grid points, and the physical values on the boundaries are obtained by extrapolating the inside values as an open free boundary condition. The initial conditions and simulation parameters are summarized in Table I. Since it is difficult to observe distortion of the contact surface directly for such a small perturbation, computational growth rates of the perturbations are evaluated by taking the mode transformation of spherical harmonics of the mass per unit area of the target instead. That is, the mass density of the target is integrated in the radial direction from the center of the target to the outer boundary across the contact surface for each polar and azimuthal direction.[14] The summed masses thus obtained as a function of the polar and azimuthal angles are expanded in the spherical-harmonic mode. Figure 1 shows a typical time evolution of the spherical-harmonic modes of the perturbations. Linear growth rates are shown as a function of polar and azimuthal mode numbers in Fig. 2.

For the theoretical analysis of the linear aspect, we introduce self-similar motion to describe the stagnation dynamics, which includes the effects of spherical geometry, acceleration, and wavelength varying in space and time.[15–17] The RT instability is investigated by using a linear eigenvalue equation for perturbations from the self-similar solution. The growth rates at maximum compression which correspond to the eigenvalues are uniquely determined by three parameters and the polar mode number (there is no explicit dependence on azimuthal mode number). The three parameters are the ratio of the contact-surface radius to the outer radius of the pusher (r_c/r_s), the density jump (ρ_f/ρ_p), and the ratio of the pressure at r_s to that at the origin $[p_0^*(r_s)/p_0^*(0)]$ (see Ref. 17 for details). We estimated them to be $r_c/r_s\sim0.62$, $\rho_f/\rho_p\sim0.1$, and $p_0^*(r_s)/p_0^*(0)\sim0.1$ from simulation results at maximum compression, and the growth rates thus obtained are shown in Fig. 2 as solid bars. There is good agreement, in both absolute value and dependence on the mode numbers; i.e., the growth rate depends only on the polar mode number n, and not on the azimuthal mode number m in spite of different geometrical shapes. It is noted that the acceleration in the analytical model at maximum compression (5.09×10^{16} cm/sec^2) is also in acceptable agreement with the acceleration in the simulations (4.36×10^{16} cm/sec^2).

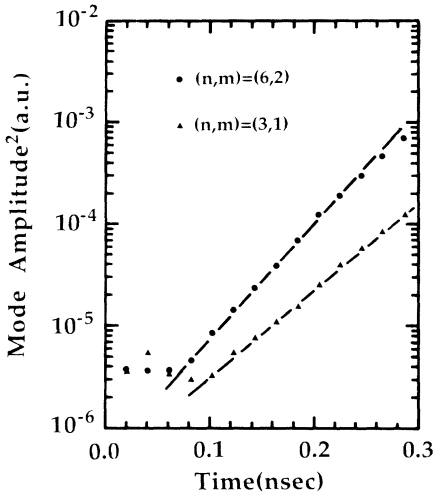

FIG. 1. Time evolution of the spherical-harmonic modes for $(n,m)=(3,1)$ and $(6,2)$.

To study the nonlinear aspect of the problem, we investigated the saturation of the exponential linear growth. Figure 3 shows the logarithm and square root of the perturbation amplitude as a function of time for $(n,m)=(6,3)$. The exponential growth saturates around $t=0.18$ nsec and is followed by the free-fall phase, in

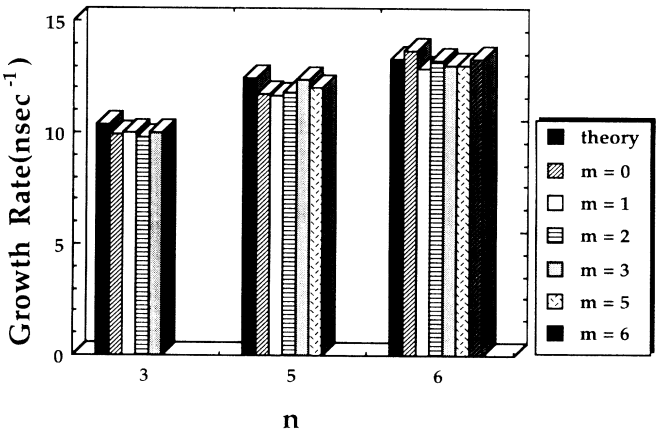

FIG. 2. Linear growth rates of simulations as a function of polar and azimuthal mode numbers with the analytic values (solid bar).

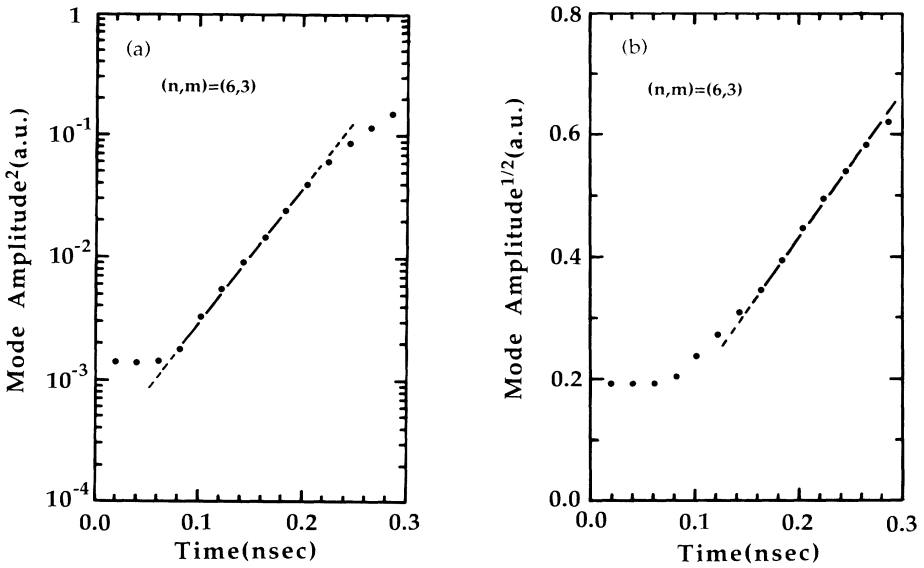

FIG. 3. Time evolution of the spherical-harmonic mode for $(n,m)=(6,3)$ in (a) logarithmic and (b) square-root plots.

which the time evolution of the amplitude is described by $\delta=\eta g t^2$. The saturation levels of exponential growth are shown as a function of mode numbers n and m in Fig. 4. The exponential growth is found to saturate around $\delta\sim\lambda_0$, where δ is the peak-to-valley amplitude of perturbations and λ_0 is estimated to be $\lambda_0=2\pi r_c(t)/n$ at saturation time. The dependence of the saturation amplitudes on the polar mode numbers is similar to the 2D results,[8] namely, for small n (~ 3) they are somewhat reduced compared with those for $n=5$ and 6. The saturation levels also have a weak dependence on the azimuthal mode numbers, in contradiction to the nondependence of the linear growth rate on them. The free-fall coefficient η is found to be nearly constant (0.8–1.1) within our present simulation parameters. Comparing with the 2D results,[8] $\delta\sim 0.35\lambda_0$ and $\eta\sim 0.2$, the 3D case indicates worse pusher-fuel mixing conditions both in larger saturation level and in faster free-fall speed. It is noted that the same features are observed in the 3D planar system,[18] but nonlinear bubble-spike structure and its feeding mechanism, which leads to a larger saturation level and faster free-fall speed, appear to be different between spherical and planar systems, as is discussed in the following.

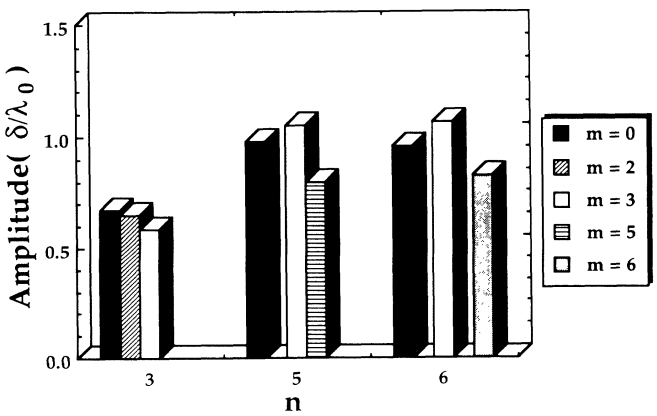

FIG. 4. Saturation amplitudes of exponential growth as a function of polar and azimuthal mode numbers.

After saturation of the exponential growth, the RT instability shifts from a linear growth phase to a free-fall phase and forms nonlinear bubble-spike structures.[14,19–21] The isovalue surfaces of the density, corresponding to the contact surface, are shown in Fig. 5 for $(n,m)=(6,3)$, showing the nonlinear bubble-spike structures of the 3D spherical system. These figures are obtained by one of the volume-rendering methods called the marching cubes algorithm.[22] During the free-fall phase, the bubbles are gradually isolated from each other and surrounded by the spikes, while the spikes are combined with each other. The bubbles float into the pusher and vortex rings are developed to feed the bubbles by blowing off the fuel into them, especially around the base of the bubbles.[18] As the pusher spikes penetrate into the center of the target, the vortex rings are tightened and enhance this feeding mechanism, and eventually lead to large saturation levels of the exponential growth. In the case of $m\sim 0$ and $m\sim n$, this feeding mechanism becomes ambiguous and the saturation amplitudes become smaller than in the other cases, because the bubbles have large structures and there are no strong vortex rings. Thus the saturation amplitudes of the exponential growth have a weak dependence on the azimuthal mode numbers.

It is noted that when we apply a perturbation of the opposite sign to the density profile near the contact surface with the same amplitude and mode numbers, the results show the same nonlinear structures in which bubbles are surrounded by spikes. Thus the bubbles surrounded by spikes are an essential feature of the 3D

FIG. 5. Three-dimensional shape of the contact surface showing nonlinear bubble-spike structures for $(n,m)=(6,3)$.

spherical system in contrast with the 3D planar system in which both bubbles surrounded by spikes and spikes surrounded by bubbles can be formed according to the initial conditions.[23]

We have presented here linear and nonlinear features of the 3D RT instability in spherically stagnating targets through numerical simulations with the 3D fluid code IMPACT-3D. The linear growth was found to be in good agreement with the analytical model, assuming the spherical symmetric dynamics to be in self-similar motion. As a nonlinear feature, the saturation amplitudes of the exponential growth were evaluated as a function of both polar and azimuthal mode numbers and the free-fall phase following the saturation was characterized by vortex rings, which tighten up and enhance the feeding of the bubbles.

We would like to thank Professor K. Mima and Dr. D. R. Bach for fruitful discussions, and Dr. R. H. Mendez and Professor S. Nakai for their interest and encouragement.

[1]Yu. F. Afanas'ev, N. G. Basov, E. G. Gamalii, O. N. Krokhin, and V. B. Rozanov, Pis'ma Zh. Eksp. Teor. Fiz. **23**, 617 (1976) [JETP Lett. **23**, 566 (1976)].

[2]J. R. Freeman, M. J. Clauser, and S. L. Thompson, Nucl. Fusion **17**, 233 (1977).

[3]S. Skupsky and K. Lee, J. Appl. Phys. **54**, 3662 (1983).

[4]M. Murakami, Ph.D. thesis, Osaka University, 1988 (unpublished).

[5]J. Gardner and S. Bodner, Phys. Rev. Lett. **47**, 1137 (1981).

[6]H. Takabe, K. Mima, L. Montierth, and R. L. Morse, Phys. Fluids **28**, 3676 (1985).

[7]S. Haan (private communication).

[8]S. Sakagami and K. Nishihara (to be published).

[9]A. Harten, J. Comput. Phys. **49**, 357 (1983).

[10]H. C. Yee, R. F. Warming, and A. Harten, J. Comput. Phys. **57**, 327 (1985).

[11]H. C. Yee, Comput. Math. Appl. **12A**, 413 (1986).

[12]T. H. Pulliam and D. S. Chaussee, J. Comput. Phys. **39**, 347 (1981).

[13]P. L. Roe, J. Comput. Phys. **43**, 357 (1981).

[14]M. H. Emery, J. P. Dahlburg, and J. H. Gardner, Phys. Fluids **31**, 1007 (1988).

[15]R. E. Kidder, Nucl. Fusion **16**, 3 (1976).

[16]D. L. Book and I. B. Bernstein, J. Plasma Phys. **23**, 521 (1980).

[17]F. Hattori, H. Takabe, and K. Mima, Phys. Fluids **29**, 1719 (1986).

[18]J. P. Dahlburg and J. H. Gardner, Phys. Rev. A **41**, 5695 (1990).

[19]C. P. Verdon, R. L. McCrory, R. L. Morse, G. R. Baker, D. I. Merion, and S. A. Orszag, Phys. Fluids **25**, 1653 (1982).

[20]D. L. Youngs, Physica (Amsterdam) **12D**, 32 (1984).

[21]K. I. Read, Physica (Amsterdam) **12D**, 45 (1984).

[22]W. Lorensen and H. Cline, Comput. Graphics **21**, 4 (1987); **21**, 163 (1987).

[23]H. E. Trease (private communication).

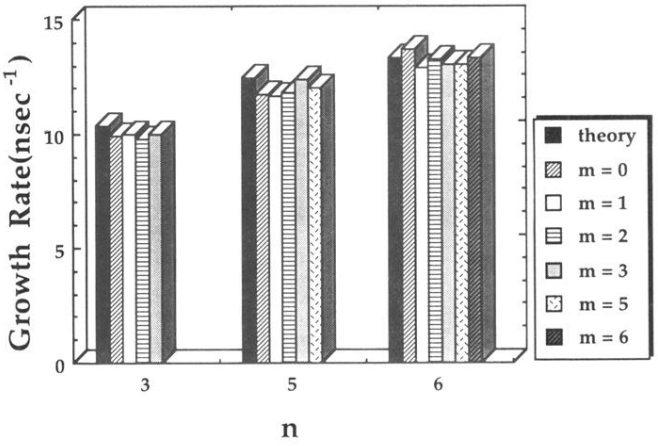

FIG. 2. Linear growth rates of simulations as a function of polar and azimuthal mode numbers with the analytic values (solid bar).

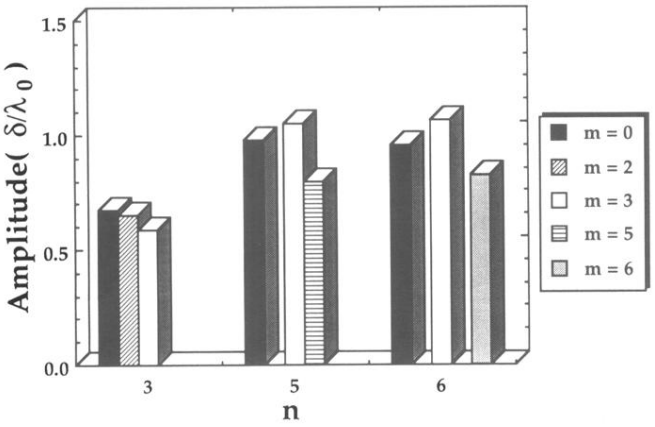

FIG. 4. Saturation amplitudes of exponential growth as a function of polar and azimuthal mode numbers.

FIG. 5. Three-dimensional shape of the contact surface showing nonlinear bubble-spike structures for $(n,m)=(6,3)$.